

Electron delocalization in gate-tunable gapless silicene

Yan-Yang Zhang,^{1,2} Wei-Feng Tsai,^{3,*} Kai Chang,¹ X.-T. An,¹ G.-P. Zhang,⁴ X.-C. Xie,² and Shu-Shen Li¹

¹*SKLSM, Institute of Semiconductors, Chinese Academy of Sciences, P.O. Box 912, Beijing 100083, China*

²*ICQM, Peking University, Beijing 100871, China*

³*Department of Physics, National Sun Yat-sen University, Kaohsiung 80424, Taiwan*

⁴*Department of Physics, Renmin University of China, Beijing 100872, China*

(Received 12 February 2013; revised manuscript received 7 September 2013; published 26 September 2013)

The application of a perpendicular electric field can drive silicene into a gapless state, characterized by two nearly fully spin-polarized Dirac cones owing to both relatively large spin-orbital interactions and inversion symmetry breaking. Here we argue that since intervalley scattering from nonmagnetic impurities is highly suppressed by time-reversal symmetry, the physics should be effectively single-Dirac-cone like. Through numerical calculations, we demonstrate that there is no significant backscattering from a single impurity that is nonmagnetic and unit-cell uniform, indicating a stable delocalized state. This conjecture is then further confirmed from a scaling of conductance for disordered systems using the same type of impurities.

DOI: 10.1103/PhysRevB.88.125431

PACS number(s): 73.21.-b, 71.23.-k

I. INTRODUCTION

It is well known that a single-cone Dirac fermion is immune to backscattering and is thus hard to be localized.^{1–4} However, graphene has two Dirac cones (valleys), as required by the fermion doubling theorem.^{1,5,6} Consequently, in the presence of impurities, the intervalley scattering from impurities cannot be strictly prohibited and this leads to remarkable backscattering, resulting in localization in two dimensions (2D).^{7–9} This is essentially different from three-dimensional topological insulators (3DTIs), with just one Dirac cone for each surface.¹⁰

Recently, silicene, which is the silicon version of graphene on a honeycomb lattice, has been an exciting subject.^{11–14} Due to its buckled structure, the spin-orbital coupling (SOC) is highly enhanced. With a perpendicular external electric field, such structure also provides the tunability of the bulk gap Δ_G .¹⁵ As the applied field increases, the gap closing and reopening indicates a topological phase transition between a 2DTI and a trivial band insulator.^{12,16–19} Exactly in the critical gapless state, where $\Delta_G = 0$, the low-energy electronic structure can be described by a massless Dirac Hamiltonian, forming two Dirac cones. The presence of various SOC interactions on the lattice results in rich spin textures around the Dirac points and eventually leads to profound behaviors in response to impurity scattering.

The most intriguing property of the gapless gated silicene, which is also the focus in this work, is the opposite spin polarization at different valleys, i.e., the valley-spin locking.^{17–19} Explicitly, the Dirac cone around the K (K') point is polarized with spin up (down), mainly originating from the intrinsic SOC between next-nearest-neighbor (NNN) sites as well as broken inversion symmetry due to the external electric field. Thus, such phase is dubbed spin-valley-polarization metal (SVPM).¹⁸ Ideally, assuming no Rashba SOC, the spin around each cone is fully polarized and, contrary to graphene, intervalley (also spin-flip) scattering from nonmagnetic impurities is strictly prohibited by time-reversal symmetry (TRS). Therefore, two Dirac cones in this system are effectively decoupled and consequently the two-component, single-flavor Dirac physics emerges. Now it is quite essential to ask if there can be any delocalized states in the strict sense under

disorder. In addition, Rashba SOC, which includes spin-flip processes, is nevertheless inevitable in realistic silicene. Can it induce intervalley scattering and lead to the breakdown of the single-Dirac-cone physics as well?

To answer these questions, in this paper, we systematically study the nonmagnetic impurity scattering problem in the gapless system, designed to capture the physics of silicene and related materials, via numerical calculations. By comparing with various typical arrangements of SOCs, we found that (1) from the quasiparticle interference (QPI) pattern associated with single impurity, within a certain region of parameter space (low energy, small Rashba SOC, and moderate impurity scattering strength) for spin-valley-polarization metal, the “unit-cell impurity” will not give rise to significant inter- or intravalley backscattering; and (2) the positive β function (defined below) in the disordered system further confirms the conclusion in (1) and suggests the existence of a truly delocalized state.

II. HAMILTONIAN AND EFFECTIVE THEORY

Silicene or the Ge, Sn, and Pb counterparts can be minimally described by a tight-binding model defined on a honeycomb lattice with energy scales $t \gg \lambda_{SO} > \lambda_R$,^{14,17,18}

$$\begin{aligned}
 H = & t \sum_{\langle ij \rangle, \sigma} c_{i\sigma}^\dagger c_{j\sigma} + i \frac{\lambda_{SO}}{3\sqrt{3}} \sum_{\langle\langle ij \rangle\rangle, \sigma\sigma'} v_{ij} c_{i\sigma}^\dagger s_{\sigma\sigma'}^z c_{j\sigma'} \\
 & - i \frac{2\lambda_R}{3} \sum_{\langle\langle ij \rangle\rangle, \sigma\sigma'} \mu_{ij} c_{i\sigma}^\dagger (\mathbf{s} \times \hat{\mathbf{d}}_{ij})_{\sigma\sigma'}^z c_{j\sigma'} \\
 & + \lambda_v \sum_{i, \sigma} \xi_i c_{i\sigma}^\dagger c_{i\sigma}.
 \end{aligned} \quad (1)$$

The first term describes the nearest-neighbor (NN) hopping, where $c_{i\sigma}^\dagger$ creates an electron at site i with spin polarization σ . The second term represents the intrinsic SOC between NNN sites, where $\mathbf{s} = (s_x, s_y, s_z)$ are the Pauli matrices for physical spins, and $v_{ij} = (\mathbf{d}_i \times \mathbf{d}_j)_z / |\mathbf{d}_i \times \mathbf{d}_j| = \pm 1$, with \mathbf{d}_i and \mathbf{d}_j the two NN bonds connecting NNN sites i and j . The third term is the NNN Rashba SOC,²⁰ where $\mu_{ij} = \pm 1$ for the A and B

sites, respectively, and $\hat{\mathbf{d}}_{ij} = \mathbf{d}_{ij}/|\mathbf{d}_{ij}|$ represent the unit vector of \mathbf{d}_{ij} which connects NNN sites i and j . The fourth term represents the staggered potential, and the strength $\lambda_v = l_z E_z$ can be tuned by a perpendicular electric field E_z because of the buckling distance l_z between two sublattices. The model parameters for silicene are $t = 1.04$ eV, $\lambda_{SO} = 4.2$ meV, $\lambda_R = 8.66$ meV, and $l_z = 0.035$ eÅ.¹⁹ Note that if we only keep the first term with $t = 2.7$ eV, then Eq. (1) simply describes undoped graphene.¹ Hereafter, we adopt t as the energy unit and lattice constant a (NNN distance) as the length unit.

Around two Dirac points at $K(K') = (\pm 4\pi/3, 0)$ in k space, the low-energy effective Hamiltonian for Eq. (1) with the basis $(\psi_{A\uparrow}, \psi_{B\uparrow}, \psi_{A\downarrow}, \psi_{B\downarrow})^T$ reads

$$H_1^\eta(\mathbf{q}) = \begin{pmatrix} h_1^\eta(\mathbf{q}) & g_1(\mathbf{q}) \\ g_1^\dagger(\mathbf{q}) & h_1^\eta(\mathbf{q}) \end{pmatrix}, \quad (2)$$

$$h_1^\eta(\mathbf{q}) = \begin{pmatrix} -\eta\lambda_{SO} + \lambda_v & \frac{\sqrt{3}}{2}t(-\eta q_x - iq_y) \\ \frac{\sqrt{3}}{2}t(-\eta q_x + iq_y) & \eta\lambda_{SO} - \lambda_v \end{pmatrix}, \quad (3)$$

$$g_1(\mathbf{q}) = \begin{pmatrix} \lambda_R(iq_x + q_y) & 0 \\ 0 & -\lambda_R(iq_x + q_y) \end{pmatrix}, \quad (4)$$

where \mathbf{q} is measured from the Dirac point, $\eta = \pm 1$ for $K(K')$ point is the valley index, and $h_1^\eta(\mathbf{q})$ is just the ideal Dirac fermion Hamiltonian for pseudospin, with Fermi velocity $\frac{\sqrt{3}}{2}t$ and mass $\lambda_v - \eta\lambda_{SO}$. Gating the system such that $\lambda_v = \lambda_{SO}$ but with $\lambda_R = 0$, the full spin polarization of the valleys can be clearly seen: At valley K , the spin-up bands are *gapless* forming a Dirac cone, in contrast to spin-down bands now separated by a gap $\Delta_G = 2|\lambda_{SO} + \lambda_v|$ and thus out of the low-energy regime; at valley K' , it is in opposite orientation due to TRS. The presence of considerable λ_R destroys this full spin polarization, but the majority around each valley does not change. Such states with two massless Dirac cones will be the main focus throughout this work. Restricting $\lambda_v = \lambda_{SO}$ (therefore, $\Delta_G = 0$) while allowing one to vary their strengths as well as the values of the Fermi level and λ_R in the system gives rise to rich physics, which reflects the interplay among spin, sublattice (pseudospin), and valley degrees of freedom under nonmagnetic impurity scattering.

III. QPI FROM SINGLE IMPURITY

The focus of the current study will be the effect of electronic scattering from impurity *potentials*. Impurity potentials can be induced by atomic substitution, surface adsorption, or by the substrate under the 2D sample. Among various origins, the adsorption of different atoms for silicene has been discussed from *ab initio* calculations recently.^{21–24} In particular, it has been found that silicene tends to adsorb adatoms (including metal atoms) more strongly than graphene. Depending on which element is concerned, the adatom can sit on the “hill,” “valley,” “bridge,” or “hollow” positions of the hexagonal ring, respectively.^{23,24}

We first investigate the scattering from a single impurity by calculating the QPI pattern.²⁵ The Green’s function for the clean system is $G^0(E, \mathbf{k}) \equiv G^0(E, \mathbf{k}, \mathbf{k}) = [(E + i\gamma)I - H(\mathbf{k})]^{-1}$, where I is the identity matrix and $\gamma \ll 1$ is the energy broadening. Here we only consider a single impurity with potential $\sim \delta(\mathbf{x})$ in a definite unit cell so that the impurity matrix

$V(\mathbf{k}_1, \mathbf{k}_2) = V$ is independent of \mathbf{k} . The impurity-induced Green’s function is expressed as

$$\delta G(E, \mathbf{k}_1, \mathbf{k}_2) = G^0(E, \mathbf{k}_1)T(E, \mathbf{k}_1, \mathbf{k}_2)G^0(E, \mathbf{k}_2). \quad (5)$$

The standard perturbation method gives²⁵

$$T(E) = [I - V\Gamma^0(E)]^{-1}V, \quad (6)$$

where $\Gamma^0(E) = \int \frac{d^2k}{(2\pi)^2} G^0(\mathbf{k}, E)$. Now the Fourier transform of the induced local density of states is

$$\delta\rho(E, \mathbf{Q}) = \frac{i}{2\pi} \int \frac{d^2k}{(2\pi)^2} g(E, \mathbf{k}, \mathbf{Q}), \quad (7)$$

where $\mathbf{Q} = \mathbf{k}' - \mathbf{k}$ and $g(E, \mathbf{k}, \mathbf{Q}) = \text{Tr}[\delta G(E, \mathbf{k}, \mathbf{k}') - \delta G^*(E, \mathbf{k}', \mathbf{k})]$. The spectrum $\delta\rho(E, \mathbf{Q})$ in Eq. (7) is called the QPI pattern, which can also be obtained experimentally from the Fourier transformation of scanning tunneling microscopy (STM) measurements.^{26,27} This pattern provides an intuitive picture of scattering processes: Significant scattering processes will manifest themselves as peaks in the QPI pattern with associated scattering momenta \mathbf{Q} .

As a warm-up, but essential, example, we start with the single-valley, single-spin, 2×2 ideal Dirac fermion Hamiltonian with just linear terms, $h_1^{\eta=1}(\mathbf{k}) = \frac{\sqrt{3}t}{2}(-k_x\tau_x + k_y\tau_y)$ [see Eq. (3)], with τ_i being the Pauli matrix acting on sublattice (pseudospin) space. The impurity potential in k space is diagonal as $V_a \equiv V_0\tau_0$, $V_b \equiv V_0\tau_3$, or their combinations with relative weight r ,

$$V = rV_a + (1-r)V_b, \quad 0 \leq r \leq 1. \quad (8)$$

The computed QPI, $\delta\rho(\mathbf{Q})$ of V_a , is plotted as the blue curve in Fig. 1(e). The curve has no significant scattering peaks, which is consistent with the well-known fact that V_a cannot induce backscattering for a massless ideal Dirac fermion.^{2–4} Notice that in the language of sublattice as pseudospin τ , V_a corresponds to a unit-cell impurity which is uniform within two sites of a unit cell. On the other hand, we also show the QPI for the “site impurity,” V_b , in Fig. 1(e) as the black curve. Two peaks associated with intravalley backscattering can be seen. This is not surprising because V_b is a mass term for ideal Dirac fermion and destroys the pseudo-TRS, leading to a tendency towards localization.² From results for an impurity with different weights of V_a and V_b also shown in Fig. 1(e), it is interesting to notice that a small weight ($r \gtrsim 20\%$) of V_a is sufficient to annihilate the significant backscattering peaks into the smooth background. In real space, an impurity with a finite V_a component corresponds to a long-range one, with a smooth potential configuration within the unit cell. Such impurities can be dominant in graphene¹ and therefore should also be easily realized experimentally for silicene. Moreover, the “hollow-type” and “bridge-type” adsorptions in silicene,^{23,24} which do not induce strong staggered potential, should also play such a role. In the rest of the paper, we will restrict ourselves to the discussions of unit-cell impurity V_a .

In the following, we will consider the full tight-binding 4×4 Hamiltonian $H(\mathbf{k})$, i.e., the k representation of H in Eq. (1). For comparison purposes, we first take parameters $\lambda_{SO} = \lambda_v = \lambda_R = 0$ such that $H(\mathbf{k})$ describes graphene without SOC. Different from the case with the ideal Dirac fermion Hamiltonian, here $H(\mathbf{k})$ has two important features:

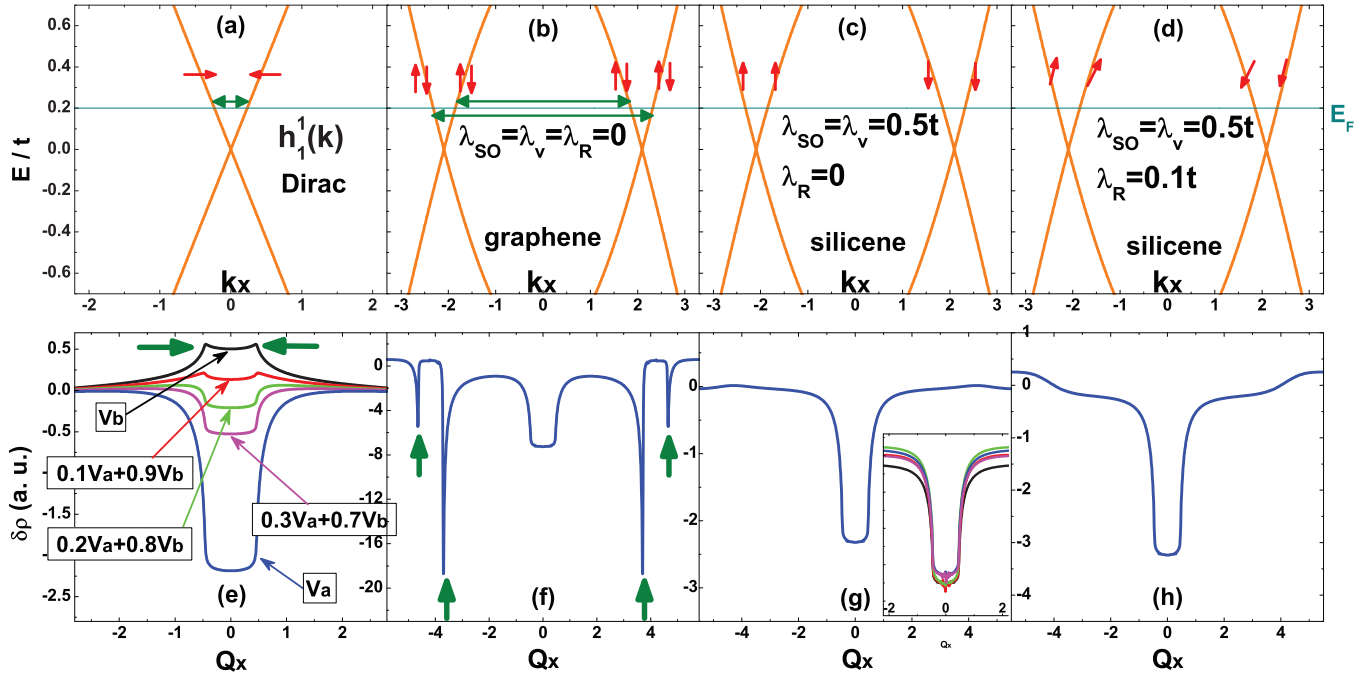


FIG. 1. (Color online) 2D dispersions $E(\mathbf{k})$ (upper row) and corresponding QPI curves $\delta\rho(\mathbf{Q})$ (lower row) for (a),(e) ideal Dirac fermion, (b),(f) graphene, and silicene with either (c),(g) $\lambda_R = 0$ or (d),(h) $\lambda_R = 0.1t$. Red arrows on dispersions illustrate the orientations of (a) pseudospins or (b)–(d) physical spins. Green thick arrows indicate significant scattering processes. Main QPI curves are plotted along the Q_x axis, while in the inset of (g), the QPI curves are plotted in different directions. All QPI curves are plotted for impurity strength $V_0 = t$, at Fermi energy $E_F = 0.2t$, with energy broadening $\gamma = 0.005t$ and 1000×1000 grid for numerical integrations.

the existence of two spins and two valleys, and higher-order corrections (trigonal warping) within each valley, as illustrated in Fig. 1(b). Given a unit-cell impurity potential,

$$V_a = V_0 s_0 \otimes \tau_0 = \text{diag}(V_0, V_0, V_0, V_0), \quad (9)$$

which is “nonmagnetic” both for physical spin s and pseudospin τ , the corresponding QPI is shown in Fig. 1(f). It has very sharp peaks associated with intervalley backscatterings between states with opposite \mathbf{k} and velocity, as indicated by the green arrows. As in ordinary orthogonal disordered systems in 2D,^{28,29} this strong backscattering is responsible for the localization in graphene^{7–9} and weak 3DTI.¹⁰ In short, the coupling between two Dirac cones (with opposite Berry curvatures)³⁰ makes the physics rather trivial.

Armed with QPI studies from the above two examples, we come to our main focus, which is gapless silicene with $\lambda_{SO} = \lambda_v = 0.5t$ for $H(\mathbf{k})$. Such large SOC is taken simply to give enough space to extract out clear physics within our numerical precisions. No qualitative difference is expected as long as Fermi energy $E_F \in (-|\lambda_{SO} + \lambda_v|, |\lambda_{SO} + \lambda_v|)$, where the SPVM picture holds.

We first consider the spin-conserved case $\lambda_R = 0$, where each valley is fully spin polarized [see Fig. 1(c)], and therefore intervalley scattering is prohibited. Indeed, with the same V_a in Eq. (9), now the QPI in Fig. 1(g) is qualitatively different from that of graphene, but similar to that of the ideal Dirac fermion [Fig. 1(e)]. Moreover, there are no significant intravalley backscattering peaks either. The intravalley features are almost isotropic in \mathbf{Q} , as shown in the inset of Fig. 1(g), even though the full band structure is anisotropic around each Dirac point. It was argued that trigonal warping would lead to

nonzero backscattering amplitude.² However, our numerical results show that such backscattering is very weak and could be immersed in the continuum background of other scattering processes, reflected by the absence of associated distinguishable peaks. Therefore, the gapless silicene with broken inversion symmetry effectively exhibits the massless Dirac fermion physics, so long as the Fermi energy is not far from the Dirac point and the impurity strength is not strong [i.e., $|E_F| + |V_0| < E$, where $E \sim O(\lambda_{SO} + \lambda_v)$, the energy scale which protects the spin-valley-polarization metal phase]. This is one of the important findings in this work. The absence of remarkable backscattering should signify a delocalized state to disorders, as will be numerically verified later.

Before entering into the discussion on disordered systems, two remarks are in order. First, in Figs. 1(c) and 1(g), with vanishing λ_R , intervalley scattering is, in fact, suppressed *a priori*. Nonzero λ_R , as is the case in silicene, makes the spin-valley polarization imperfect [see Fig. 1(d)]. However, as shown in Fig. 1(h), it is remarkable to see that such Rashba term does not give rise to a significant intervalley scattering, and thus the effective “single-valley Dirac physics” remains intact. This can be due to the following two intuitive reasons: (1) The NNN Rashba interaction makes no contribution at K (K') points and thus its effect is also expected to be small around K (K') points; (2) the full backward scattering, which relates intervalley points, i.e., time-reversal partners (still with opposite spin polarizations under Rashba interaction), is difficult to happen through *nonmagnetic* impurity.

Second, further increasing a parameter such as E_F , impurity strength V_0 , or λ_R in the system is expected to enhance

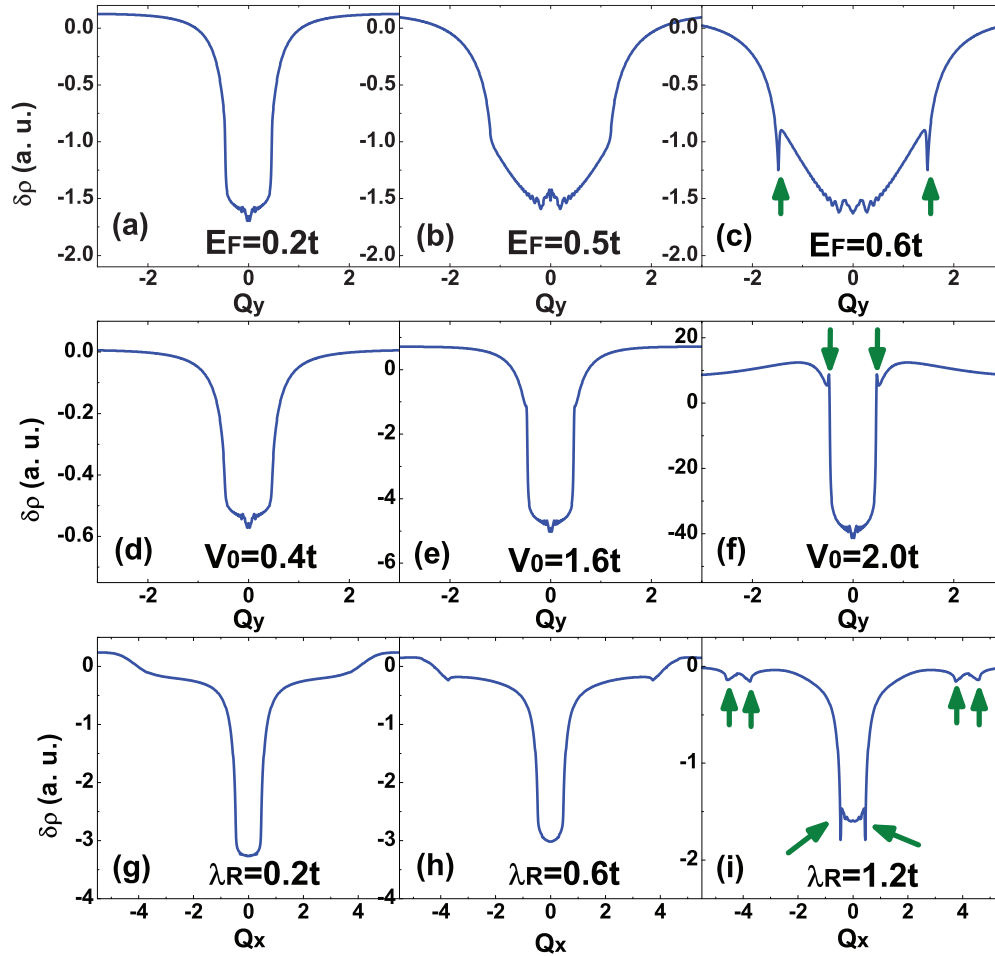


FIG. 2. (Color online) QPI pattern for silicene with different Fermi energies E_F , impurity strengths V_0 , and Rashba SOC λ_R . (a)–(c) $V_0 = t$ and $\lambda_R = 0$; (d)–(f) $E_F = 0.2t$ and $\lambda_R = 0$; (g)–(i) $E_F = 0.2t$ and $V_0 = t$. The scanning angle is chosen along the Q_y axis from (a) to (f), where possible intravalley backscattering reaches its maximum amplitude,² and along Q_x axis from (g) to (i) for the detection of possible intervalley scattering. All other parameters are the same as Fig. 1(g).

intra- and intervalley scattering processes due to unavoidable contributions from higher-order corrections and spin/valley mixing. Indeed, as clearly shown in Fig. 2, the QPI pattern changes at some point, indicating a transition from a delocalized to localized state beyond effective single-valley Dirac physics. For instance, in the case of very strong λ_R in Fig. 2(i), although two states $|\mathbf{k}\rangle$ and $|\mathbf{-k}\rangle$ in different valleys (with exactly opposite spin orientations) cannot be coupled by a nonmagnetic impurity, the spin orientations in their neighborhoods will not be exactly opposite. Thus, an intervalley backscattering can be allowed due to the energy broadening γ .

IV. SCALING OF CONDUCTANCE: MULTIPLE IMPURITIES

So far, the scattering from a single impurity has been investigated. If the backscattering is effectively ignorable, does this really lead to a delocalized state in disordered gapless silicene with unit-cell impurities? To confirm that it does, we perform a standard numerical scaling for disordered silicene. Disorder is added to the Hamiltonian (1) as $\sum_{i,\sigma} \epsilon_i c_{i\sigma}^\dagger c_{i\sigma}$,

where ϵ_i is a random number uniformly distributed within $(-W/2, W/2)$. Here, ϵ_i is independent of spin due to TRS. If ϵ_i is further identical for two sites in each unit cell, then it corresponds to unit cell impurities V_a . In realistic silicene material, such impurities can be long-range impurities as in graphene,¹ or the hollow and bridge types of adsorbed impurities as reported in Refs. 23 and 24. The intrinsic conductance g is defined as $1/g = 1/g_L - 1/N_c$, where g_L is the two-terminal quantum conductance, N_c is the number of propagating channels, and $1/N_c$ is the contact resistance.³¹ This g is suitable for a numerical scaling,^{9,32}

$$\beta = \frac{d \langle \ln g \rangle}{d \ln L}, \quad (10)$$

where $\langle \cdot \rangle$ is the average over random ensemble, and L is the spatial size of the sample with a fixed ratio of length and width. This scaling function β is used as a criteria: $\beta < 0$ and $\beta > 0$ correspond to localized and delocalized states, respectively.

In Fig. 3, we plot $\langle \ln g \rangle$ as a function of size L (in logarithmic scale), where the slope represents β . It can be seen from Figs. 3(a) and 3(b) that for unit-cell impurities, apart from some fluctuations due to the smallness of conducting channels, $\langle \ln g \rangle$ is clearly increasing with increasing L , suggesting a

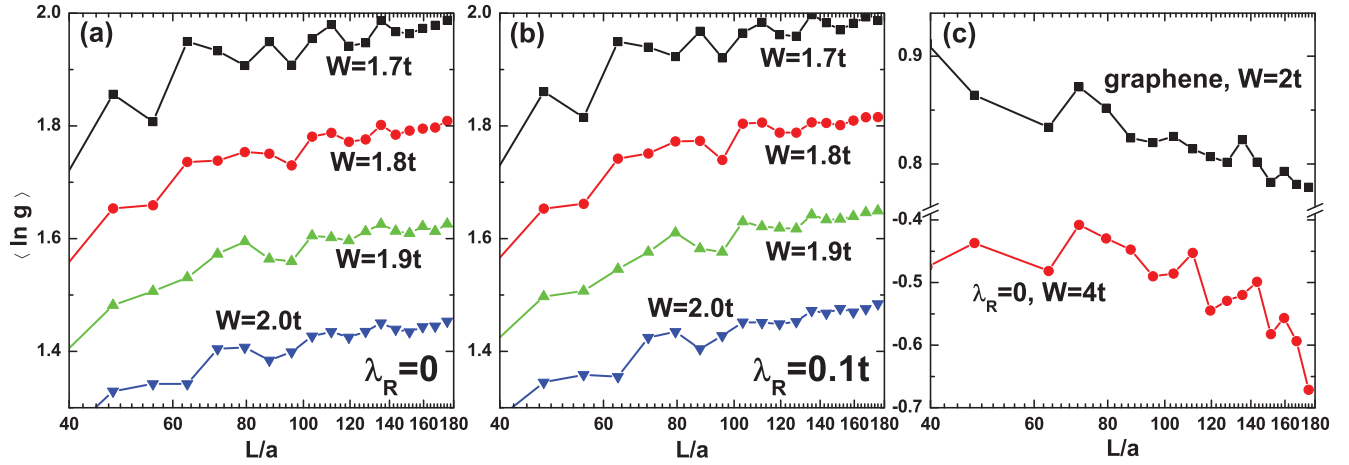


FIG. 3. (Color online) Typical conductance as a function of the system size (in logarithmic scale). (a) $\lambda_{SO} = \lambda_v = 0.5t$, $\lambda_R = 0$; (b) $\lambda_R = 0.1t$; (c) Two examples of localization: graphene with $W = 2t$ (black line) and silicene with $\lambda_{SO} = \lambda_v = 0.5t$, $\lambda_R = 0$, under strong disorder $W = 4t$ (red line). Each dot is the average over 2000 disorder samples with unit-cell impurities.

delocalized state with $\beta > 0$. These are consistent with our results of the absence of significant backscattering from the single-impurity study, further confirming the robustness of the effective single-valley Dirac physics. Note that this is totally different from the case of graphene with the $W = 2t$ [black curve in Fig. 3(c)], where the slope is negative. It has been found that for graphene, even long-range impurities cannot maintain a fully delocalized state with $\beta > 0$ because of inevitable intervalley scattering.⁹ Of course, as in any lattice models, sufficiently strong disorder, for instance with $V_0 \gg O(\lambda_{SO} + \lambda_v)$, will eventually localize all the electrons, as the red curve in Fig. 3(c) shows. Therefore, it is natural to expect rich localization-delocalization transition behavior in the parameter space spanned by E_F , W , λ_R , and λ_{SO} ($=\lambda_v$). More details of such localization-delocalization transition, e.g., the universality, critical exponents, and global phase diagram, will be discussed elsewhere.

Delocalized bulk states in the doped Kane-Mele model with nontrivial Z_2 topological nature were found in Ref. 33. In that case, delocalized states can only appear when large (comparable to E_F) and inversion-broken NN Rashba SOC is nonzero, making the system truly *symplectic*. Otherwise, the system is just decoupled into two gapped *unitary* subsystems, namely, two massive Dirac cones around K and K' , where no states with $\beta > 0$ can be observed.³³ This is indeed reasonable, as a gapped Dirac cone has serious backscattering.² In our case, however, the physics behind delocalization lies on either independent unitary subsystems, each of which owns a massless Dirac cone (zero NNN Rashba SOC), or symplectic subsystems with two nearly independent gapless Dirac cones (nonzero NNN Rashba SOC). The Dirac cones are already nondegenerate with almost fully spin polarization (along the z axis) as long as the inversion-symmetric, NNN λ_R interaction is small.

V. DISCUSSION AND CONCLUSION

The essence of this work is to reveal the physics behind the delocalization phenomenon, which can be understood from the picture of effectively decoupled gapless Dirac cones. This

picture is valid in certain parameter ranges. Here we emphasize again the relevant energy scales important to any experimental demonstration for the delocalization in silicene, such as the presence of a robust Dirac point and linear dispersion in STM or the weak antilocalization in the magnetoresistance measurement. First, the gapless condition $\lambda_v = l_z E_z = \lambda_{SO}$ gives the critical electric field $E_z = \lambda_{SO}/l_z \sim 0.12 \text{ V \AA}^{-1}$, which is experimentally achievable. In this case, the half width of the energy window for spin-valley locking is $|\lambda_{SO} + \lambda_v| = 2|\lambda_{SO}| \sim 8.4 \text{ meV}$. This range can be even larger in the Ge, Sn, or Pb counterpart.¹⁹ On the other hand, such energy window is still small enough to keep the dispersion of Dirac fermions linear. Although NNN Rashba SOC breaks the perfect spin-valley locking, $\lambda_R = 8.66 \text{ meV}$ is less than 1% of t , and therefore this effect is very weak.

In summary, we reveal the essential transport properties via numerical simulations on a critically gated buckled honeycomb structure of silicene (and also suitable for Ge, Sn, and Pb counterparts) under nonmagnetic impurity scattering. In particular, as long as $|E_F| + |V_0| < E$, with E an energy scale of the order of $\lambda_{SO} + \lambda_v$, we find the following: (1) QPI by a single unit-cell impurity shows no significant backscattering, suggesting an effective *single-valley* Dirac physics, in spite of weak trigonal warping. (2) The robustness of such delocalized state is further confirmed by the positiveness of the β function for a disordered system, even in the presence of Rashba SOC. Our finding sheds light on constructing high-mobility silicene-based electronic devices. Moreover, we believe our result is also insightful to relevant systems such as a 2D MoS₂ (Ref. 34) and a cold-atom system with arranged SOC.³⁵

ACKNOWLEDGMENTS

Y.Y.Z. thanks Q. F. Sun, H. Jiang, and H. W. Liu for beneficial discussions. This work was supported by NSFC (Grant No. 11204294) and 973 Program (Project No. 2013CB933304). W.F.T. is supported by the NSC in Taiwan under Grant No. 102-2112-M-110-009.

*To whom correspondence should be addressed: wftsai@mail.nsysu.edu.tw

- ¹A. H. Castro Neto, F. Guinea, N. M. R. Peres, K. S. Novoselov, and A. K. Geim, *Rev. Mod. Phys.* **81**, 109 (2009).
- ²T. Ando, T. Nakanishi, and R. Saito, *J. Phys. Soc. Jpn.* **67**, 2857 (1998).
- ³K. Nomura, M. Koshino, and S. Ryu, *Phys. Rev. Lett.* **99**, 146806 (2007).
- ⁴J. H. Bardarson, J. Tworzydło, P. W. Brouwer, and C. W. J. Beenakker, *Phys. Rev. Lett.* **99**, 106801 (2007).
- ⁵K. S. Novoselov, A. K. Geim, S. V. Morozov, D. Jiang, Y. Zhang, S. V. Dubonos, I. V. Grigorieva, and A. A. Firsov, *Science* **306**, 666 (2004).
- ⁶Y. Jiang, T. Low, K. Chang, M. I. Katsnelson, and F. Guinea, *Phys. Rev. Lett.* **110**, 046601 (2013).
- ⁷A. F. Morpurgo and F. Guinea, *Phys. Rev. Lett.* **97**, 196804 (2006).
- ⁸A. Altland, *Phys. Rev. Lett.* **97**, 236802 (2006).
- ⁹Y.-Y. Zhang, J.-P. Hu, B. A. Bernevig, X. R. Wang, X. C. Xie, and W. M. Liu, *Phys. Rev. Lett.* **102**, 106401 (2009).
- ¹⁰See, for instance, M. Z. Hasan and C. L. Kane, *Rev. Mod. Phys.* **82**, 3045 (2010), and references therein.
- ¹¹B. Lalmi, H. Oughaddou, H. Enriquez, A. Kara, S. Vizzini, B. Ealet, and B. Aufray, *Appl. Phys. Lett.* **97**, 223109 (2010).
- ¹²C.-C. Liu, W. Feng, and Y. Yao, *Phys. Rev. Lett.* **107**, 076802 (2011).
- ¹³B. Feng, Z. Ding, S. Meng, Y. Yao, X. He, P. Cheng, L. Chen, and K. Wu, *Nano Lett.* **12**, 3507 (2012).
- ¹⁴C.-C. Liu, H. Jiang, and Y. Yao, *Phys. Rev. B* **84**, 195430 (2011).
- ¹⁵N. D. Drummond, V. Zolyomi, and V. I. Fal'ko, *Phys. Rev. B* **85**, 075423 (2012).
- ¹⁶C. L. Kane and E. J. Mele, *Phys. Rev. Lett.* **95**, 146802 (2005); **95**, 226801 (2005).
- ¹⁷M. Ezawa, *New J. Phys.* **14**, 033003 (2012).
- ¹⁸M. Ezawa, *Phys. Rev. Lett.* **109**, 055502 (2012).
- ¹⁹W.-F. Tsai, C.-Y. Huang, T.-R. Chang, H. Lin, H.-T. Jeng, and A. Bansil, *Nat. Commun.* **4**, 1500 (2013).
- ²⁰An NN Rashba SOC term could also be induced by inversion symmetry breaking in the gated silicene. However, such coupling is estimated to be much smaller than λ_R and becomes zero at our focused gapless state.¹⁸ Thus, one can safely ignore it.
- ²¹R. Quhe, R. Fei, Q. Liu, J. Zheng, H. Li, C. Xu, Z. Ni, Y. Wang, D. Yu, Z. Gao, and Jing Lu, *Sci. Rep.* **2**, 853 (2012).
- ²²X. Lin and J. Ni, *Phys. Rev. B* **86**, 075440 (2012).
- ²³H. Sahin and F. M. Peeters, *Phys. Rev. B* **87**, 085423 (2013).
- ²⁴J. Sivek, H. Sahin, B. Partoens, and F. M. Peeters, *Phys. Rev. B* **87**, 085444 (2013).
- ²⁵Q.-H. Wang and D.-H. Lee, *Phys. Rev. B* **67**, 020511(R) (2003).
- ²⁶J. E. Hoffman, K. McElroy, D.-H. Lee, K. M. Lang, H. Eisaki, S. Uchida, and J. C. Davis, *Science* **297**, 1148 (2002).
- ²⁷P. Roushan, J. Seo, C. V. Parker, Y. S. Hor, D. Hsieh, D. Qian, A. Richardella, M. Z. Hasan, R. J. Cava, and Ali Yazdani, *Nature (London)* **460**, 1106 (2009).
- ²⁸P. W. Anderson, *Phys. Rev.* **109**, 1492 (1958).
- ²⁹P. A. Lee and T. V. Ramakrishnan, *Rev. Mod. Phys.* **57**, 287 (1985).
- ³⁰D. Xiao, W. Yao, and Q. Niu, *Phys. Rev. Lett.* **99**, 236809 (2007).
- ³¹D. Braun, E. Hofstetter, G. Montambaux, and A. MacKinnon, *Phys. Rev. B* **55**, 7557 (1997).
- ³²K. Slevin, P. Markoš, and T. Ohtsuki, *Phys. Rev. Lett.* **86**, 3594 (2001).
- ³³M. Onoda, Y. Avishai, and N. Nagaosa, *Phys. Rev. Lett.* **98**, 076802 (2007).
- ³⁴D. Xiao, G.-B. Liu, W.-X. Feng, X.-D. Xu, and W. Yao, *Phys. Rev. Lett.* **108**, 196802 (2012).
- ³⁵N. Goldman, A. Kubasiak, A. Bermudez, P. Gaspard, M. Lewenstein, and M. A. Martin-Delgado, *Phys. Rev. Lett.* **103**, 035301 (2009).